Uludağ University Journal of The Faculty of Engineering, Vol. 30, No. 3, 2025 RESEARCH

DOI: 10.17482/uumfd.1601353

LEVERAGING AI TO IDENTIFY SILT ACCUMULATION AND BLOCKAGE IN COLLECTION SYSTEMS

Mehmet B. Ercan [*]

Received: 14.12.2024; revised: 09.09.2025; accepted: 14.09.2025

Abstract: Solid waste accumulation in wastewater collection systems poses significant challenges, leading to blockages, reduced flow capacity, and an increased risk of Separate or Combined Sewer Overflows (SSO or CSO), threatening public safety through flooding and pathogen contamination. Proactive detection of such buildups is critical, yet current automated methods are limited to academic studies that rely solely on depth data, lacking velocity information essential for determining silt depth accurately. This study addresses this gap by training a Deep Convolutional Neural Network (CNN) on depth-velocity scatter plots generated from 1,482,000 simulations using the Storm Water Management Model (SWMM), producing 82,482 labeled plots of varying silt accumulation levels. The CNN achieved 99% accuracy (for solid content predictions with deviations of up to 10%) on test data and was further validated with three real-world experiments using 20 cm pipes, where blockages were predicted within 0 cm, 0.3 cm, and 1.5 cm of actual conditions. These findings demonstrate CNNs as an effective tool for identifying silt accumulation, offering a faster and more precise alternative to traditional methods, with the potential to enhance maintenance and reduce system failure risks. Further research is needed to optimize the model for broader real-world applications.

Keywords: Sanitary Sewer and Stormwater Collection Systems, Silt Accumulation, Artificial Intelligent, Convolutional Neural Network

Yapay Zeka İle Atıksu Toplama Sistemlerinde Katı Madde Birikiminin ve Tıkanıklığın Tespit Edilmesi

Öz: Atıksu toplama sistemlerinde katı madde birikimi, tıkanmalara, akış kapasitesinin azalmasına ve Ayrık veya Birleşik Kanal Taşmaları (SSO veya CSO) riskinin artmasına yol açarak sel ve patojen bulaşması gibi halk sağlığını tehdit eden ciddi sorunlara neden olmaktadır. Bu tür birikimlerin erken tespiti kritik öneme sahip olsa da mevcut otomatik yöntemler, yalnızca derinlik verilerine dayanan ve hız bilgisi eksikliği nedeniyle tutarsız sonuçlar veren akademik çalışmalarla sınırlıdır. Bu çalışmada, Yağmur Suyu Yönetim Modeli (SWMM) ile oluşturulan 1.482.000 simülasyon sonucunda derinlik-hız dağılım grafiklerinden 82.482 etiketli silt birikim seviyesi grafiği kullanılarak bir Derin Evrişimli Sinir Ağı (CNN) eğitilmiştir. CNN, test verilerinde (katı madde miktarı tahminlerinde %10'a kadar olan sapmalarla) %99 doğruluk oranına ulaşmış ve 20 cm çapındaki borularla yapılan üç gerçek deney ile doğrulanmıştır. Bu deneylerde, tıkanmalar gerçek koşullara sırasıyla 0 cm, 0,3 cm ve 1,5 cm yakınlıkta tahmin edilmiştir. Sonuçlar, CNN'in silt birikimini tespit etmede etkili bir araç olduğunu, geleneksel yöntemlere göre daha hızlı ve hassas bir çözüm sunduğunu, bakım süreçlerini iyileştirme ve sistem arıza risklerini azaltma potansiyeline sahip olduğunu göstermektedir. Ancak, modelin daha geniş kapsamlı gerçek hayattaki uygulamalar için optimize edilmesine ve ek araştırmalara ihtiyaç duyulmaktadır.

Anahtar Kelimeler: Atıksu ve Yağmur suyu Toplama Sistemleri, Katı Madde Birikimi, Yapay Zeka, Evrişimli Sinir Ağı

[*] İnönü University, Faculty of Engineering, Department of Civil Engineering, Battalgazi Malatya 44210, Türkiye
Corresponding Author: Mehmet B. Ercan (mehmetb.ercan@inonu.edu.tr)

1. INTRODUCTION

Solid waste accumulation in wastewater collection systems continues to be a persistent challenge that significantly disrupts the functionality of these infrastructures (Türk et al., 2022; Ebtehaj et al., 2015). Sediment and domestic solid waste can cause blockages, reducing flow capacity and increasing the risk of Sanitary Sewer Overflows (SSOs) and Combined Sewer Overflows (CSOs). These SSO and CSO events pose serious threats to public health by causing flooding and contaminating water sources with harmful pathogens (Muttil et al., 2023; Li et al., 2010). The rapid growth of urban populations and the increasing frequency of extreme weather events due to climate change further exacerbate these risks, making the proactive management of solid waste accumulation an urgent necessity (Berggren et al., 2012; Semadeni-Davies et al., 2008).

Traditional methods for detecting solid waste accumulation, such as Manning's graph, offer limited insights as they rely on manual interpretation and engineering judgment (Vitorino et al., 2014; Ebtehaj et al., 2015). Recent studies on using real-time sensors to detect channel blockages automatically focus solely on depth sensors (Faris et al., 2024; Li et al., 2023), which may misinterpret full pipe flow as a blockage. Therefore, the effective integration of depth and velocity variables in Manning's graph for automatically detecting blockages or sediment accumulation in sewer systems has not yet been implemented.

The Manning equation (Manning, 1891) calculates the water flow velocity based on the channel's roughness, slope, and hydraulic radius. When engineers overlay the graph generated using Manning's equation onto the depth and velocity distribution graph, they can make inferences based on their engineering experience about issues on the downstream or upstream side of the wastewater channel, or whether sediment has accumulated (Stevens and Sands, 1995). Since these graphs require engineers to infer flow conditions and sediment dynamics, automating this interpretation would provide rapid, unbiased, and scalable AI-backed decision support.

The field requires more efficient, automated detection methods, but progress has been limited (Faris et al., 2024; Li et al., 2023). Depth–velocity scatter plots offer insights into wastewater-system conditions, so an AI-based approach to automatically detect conditions would benefit the water resources industry. Given that these plots are images, a Convolutional Neural Network (CNN) would be particularly effective.

CNNs are specialized deep learning models that process matrix-like data, such as images and videos. These models use multiple layers of convolutional filters to learn spatial hierarchies of features from the input data automatically and adaptively (LeCun et al., 2015). A key advantage of CNNs over traditional deep learning models is their ability to reduce the number of parameters through weight sharing, which enhances training efficiency and reduces the likelihood of overfitting (Krizhevsky et al., 2012). These features make CNNs suitable for various applications, including image and video recognition, medical image analysis, and natural language processing (Goodfellow et al., 2016). Additionally, CNNs have been used to detect defects based on images captured by robots in wastewater channel systems (Tan et al., 2021; Xie et al., 2019; Guo et al., 2009). However, CNNs or any image recognition AI have never been used to detect sediment accumulation and blockage.

In this study, we generated approximately 1.5 million Storm Water Management Models (SWMM) to comprehensively replicate real-world conditions and produce depth and velocity data. From these simulations, we created 82,482 depth–velocity scatter plots, which were used to train a Deep Convolutional Neural Network (CNN) model to predict solid waste levels in the wastewater collection system.

This approach leveraged the SWMM to simulate data at scale, ensuring that the resulting CNN model could learn from a diverse set of scenarios and generalize to real-world conditions. By systematically varying channel roughness, slope, and hydraulic radius, we captured a wide

range of flow regimes and sediment dynamics, enabling robust detection of solid waste accumulation. The trained CNN demonstrates strong performance across multiple validation scenarios and offers a scalable, automated tool for water resources management. This work lays the groundwork for integrating AI-driven analysis into routine infrastructure monitoring, potentially reducing downtime and maintenance costs while improving public health outcomes.

2. MATERIALS AND METHODS

To effectively represent all potential real-life conditions, this study developed a variety of SWMM model combinations based on the set of conditions explained in Section 2.2. Each model was simulated until the system reached a steady state, with the model carefully analyzed and processed to eliminate oscillations that could hinder steady-state conditions. Subsequently, depth and velocity scatter plots were generated to illustrate the changes and behaviors within the flow system caused by silt accumulations. Each model produced a single point on the scatter plot, as the steady-state condition resulted in a single velocity and depth value. The number of points increased with additional models running under different upstream conditions. These scatter plots were then utilized as input for training the CNN model.

2.1. Creating Base SWMM Model

Figure 1 illustrates the profile and basic structure of the SWMM model, developed based on experimental studies focused on channel blockages, solid material accumulation, and transport (Montes et al., 2020; Vongvisessomjai et al., 2010; Enfinger et al., 2004; Ghani, 1993; Perrusquia, 1992; El-Zaemey, 1991). The model includes two additional pipes (C1 and C3) to accurately represent flow conditions on both the upstream and downstream sides of the Cmeter pipe. The channel lengths and depths are designed by Turkish regulations (Regulation on Wastewater Collection and Disposal Systems, 2017). The standard pipe length is 70 meters, while pipes with diameters greater than 120 cm are modeled at 100 meters. Manhole depths are adjusted based on the pipe diameter and standardized at 2.7 meters from the crown of the pipe. This study focuses on circular conduits and does not examine silt accumulation in other conduits.

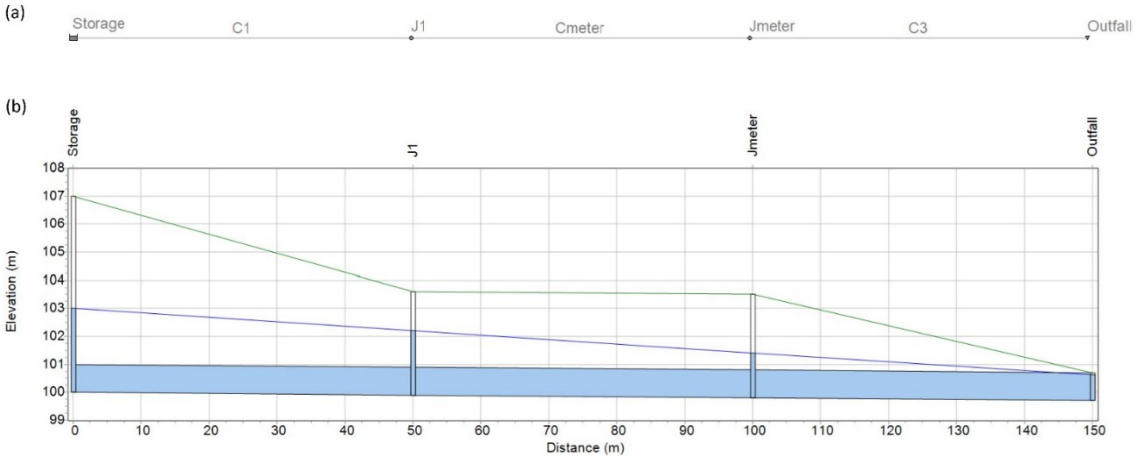


Figure 1:
Base SWMM Model;
a. *Plan view* ***b.*** *Profile view*
b.

2.2. Creating SWMM Model Variations

A total of 1,482,000 unique SWMM models were generated by varying pipe diameters, slopes, upstream and downstream flow conditions, and silt depths (Table 1). Pipe diameters ranged from 20 cm to 200 cm, increasing in 10 cm increments. Silt depths were defined as percentages of the pipe diameter, with 13 levels ranging from 0% to 60%. Slopes were distributed across 10 equal intervals within the minimum and maximum allowable values based on regulations.

Upstream storage depths were divided into 15 equal increments up to conduit diameter, followed by another 15 increments extending up to 200 cm above the flooding point, accounting for varying flood conditions. For example, Table 1 shows that storage depth starts at 6 cm, including 5 cm of silt depth and approximately 1 cm of increment. After the conduit diameter of 20 cm, increments increase to reach 490 cm in 15 steps. The maximum value, 490 cm, is calculated as 2 meters above the manhole level (20 cm conduit + 270 cm manhole depth + 200 cm additional height).

For downstream boundary conditions, depths increased in 10 equal increments up to the sensor pipe diameter, followed by another 10 increments up to the flooding point at the sensor location. The energy slope, used to determine downstream boundary limits, was assumed equal to the conduit slope under normal conditions and twice the conduit slope for surcharged conditions. The example variable values shown in Table 1 show that downstream (outfall) boundary conditions began at 5 cm (representing zero water level at the outfall with 5 cm of silt) and increased to 48 cm in 10 steps (5 cm silt depth, 20 cm conduit diameter, and 23 cm energy loss from the outfall to the sensor location). From 48 cm, the depths were further increased to 341 cm in 10 steps (5 cm silt depth, 20 cm conduit diameter, 46 cm energy loss, and 270 cm manhole depth to the crown of the pipe).

Table 1. Variations in the SWMM Model

Parameters	Explanation for Variable Values	Variable Values
Diameter (cm)	20 to 200 in 10 cm increments	20, 30, ..., 190, 200
Silt Depth (%)	13 different accumulated silt depths ranging from 0% to 60% of conduit diameter	0, 5, 10, 15, 20, 25,30, 35, 40, 45, 50, 55, 60
Slope (%)	10 equal intervals between minimum and maximum allowed slopes (conduit size changes min and max slope values)	E.g. For conduits smaller than 30 cm: 0.3, 1.0, ..., 6.0, 6.7
Storage Depth (cm)	15 equal increments up to the conduit diameter, followed by another 15 increments up to 470 cm + conduit size	E.g. For 20 cm conduits and 5 cm silt accumulation: 6, 7, …, 19, 20, 21, 54, 88, …, 456, 490
Outfall Boundary (cm)	10 equal increments up to the sensor conduit diameter, followed by another 10 increments up to the sensor flooding point	E.g. For 20 cm conduits, 5 cm silt accumulation, 7000 cm conduit length and 0.0033 slope (23 cm drop): 5, 10, …, 43, 48, 81, 113, …, 308, 341

Using the variations described, 19 conduit sizes, 13 silt depths, 10 conduit slopes, 20 downstream depths, and 30 upstream depths were established as the parameter set. These values

were determined through extensive trial and error to optimize model performance within the limits of available computing power. The combination of these parameters resulted in 1,482,000 unique SWMM models, each simulated until reaching steady-state conditions.

2.3. Creating Scatter Plots for Artificial Intelligence Model

When the SWMM models reached steady-state conditions, a single steady-state velocity and depth value was extracted at the sensor location for each model. These values were used to generate scatter plots. Figure 2 illustrates example scatter plots for a specific scenario: 60 cm conduit diameter, 6 cm silt depth, 0.0104 slope, and a 65 cm outfall boundary condition (depth above the outfall invert). In Figure 2.a, the blue data points represent 30 different upstream conditions. In Figures 2.b and 2.c, the number of points varies depending on the available depth conditions within the limits described below.

Gray lines indicate pipe diameter, green lines denote the ground (shown only in Figure 2.a), and red lines represent conduit slopes, helping the CNN model predict sediment depths accurately. As AI input plots, Labels, numbers, and coordinate lines were omitted to simplify AI training. Further, the figure resolutions were reduced to 126x123 pixels to address memory constraints during data loading, which slightly lengthened the training process but did not significantly affect model performance. Further reducing the resolution degraded figure quality and negatively impacted the AI model training.

The X and Y coordinate ranges were standardized to maintain consistency and prevent data misinterpretation. For Figures 2.b and 2.c, depth ranges were set between -0.1 and 3 meters, and velocity ranges between -3 and 5 m/s. For Figure 2.a, depth ranges were between -0.1 and 5 meters, and velocity ranges between -6 and 8 m/s.

Three figure categories were created to approximate real-life conditions:

- **All Depth Conditions (Figure 2.a):** Includes both dry and wet scenarios.
- **Dry and Slightly Wet Conditions (Figure 2.b):** Depths below the conduit diameter.
- **Likely Dry Conditions (Figure 2.c):** Depths between 20% and 70% of the conduit diameter.

In total, 82,482 plots were generated: 46,930 for all depth conditions (Figure 2.a), 19,749 for dry and slightly wet conditions (Figure 2.b), and 15,803 for likely dry conditions (Figure 2.c). The fewer number of figures for dry and slightly wet conditions (Figure 2.b) and likely dry conditions (Figure 2.c) was due to the SWMM model parameter set that did not produced any depth values within the limits explained above.

As explained above, all data were synthetically generated; therefore, a detailed investigation of the CNN model's input data was initially considered unnecessary. However, we manually reviewed all 46,930 plots—for all depth conditions—to identify any inconsistencies in how the data points were distributed. During this process, we identified several cases where the SWMM model had not reached steady-state conditions. To resolve this, we increased the simulation run time, reduced the Head Convergence Tolerance, shortened the routing time step, and increased the maximum number of Dynamic Wave trials. These adjustments were applied across all 1,482,000 SWMM model runs, ensuring steady-state conditions were met and that the input data quality for the CNN model was robust.

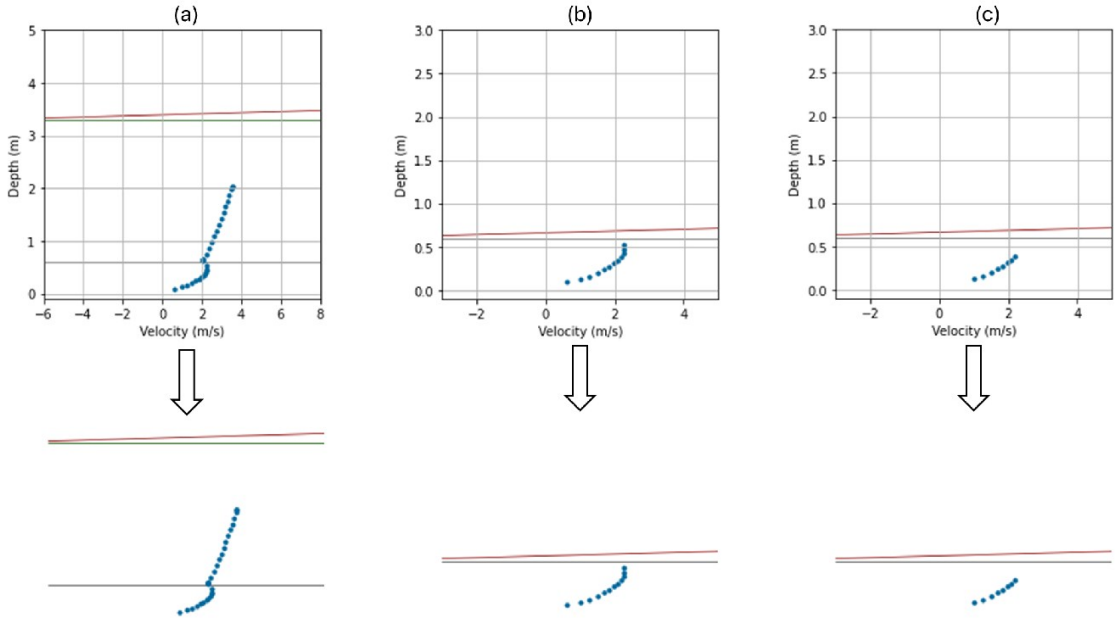


Figure 2:
Scatter Plots for AI Training;
a. *All Depth Condition* ***b.*** *Dry and Slightly Wet Condition* ***c.*** *Likely Dry Condition*

3. ARTIFICIAL INTELLIGENCE MODEL AND TRAINING

A Deep Convolutional Neural Network (CNN) model was implemented as the AI model using Python's TensorFlow libraries (Raschka and Mirjalili, 2019). There are different versions of CNN available (Khan et al., 2020; Rawat and Wang, 2017). However, we did not use different versions of the CNN method as Raschka and Mirjalili (2019)'s method was readily available, and the scope of this study was to show applicability of graph reading for silt detection in the collection systems. The dataset of 82,482 plots was split for training, validation and testing: every 41st plot was used for validation, every 11th plot for testing, and the remaining plots for training (Table 2). This resulted in 73,155 training plots, 7,498 validation plots, and 1,829 test plots. Table 2 indicates good distribution of silt depth (dependent data) as standard deviation is within 5.7% of the mean throughout training, validation and test data.

Table 2. Independent and Dependent Data Statistics

		Independent (X) Data		Dependent (Y) Data		
Data Type	Count	Resolution	Colors	Unique Count	Mean	Standard Deviation
Training	73155	123x126	RGB	13	5627.3	324.7
Validation	7498	123x126	RGB	13	576.8	33.2
Test	1829	123x126	RGB	13	140.7	8.0

The cross-entropy loss function was employed to classify 13 sediment depth categories, ranging from 0% to 60% of the conduit size (see Table 1 variable values). This approach

penalizes errors, encouraging the model's outputs to align closely with the true class labels. As the loss function value decreases, the CNN model's predictive accuracy improves (Goodfellow et al., 2016).

Figure 3 illustrates the training and testing accuracy history of the CNN model. The first 50 epochs represent training and testing accuracy achieved with a learning rate of 0.001. This is followed by the first fine-tuning phase with a learning rate of 0.0001 (highlighted in light turquoise for 10 epochs) and the second fine-tuning phase with a learning rate of 0.00001 (highlighted in darker turquoise for the final 5 epochs).

Accuracy improvements were most pronounced during the initial epochs of the first training phase, significantly decreasing after the first 8 epochs. Similarly, during the first fine-tuning phase, accuracy increased rapidly over the first few epochs before slowing down. While validation accuracy improved throughout training, it did not reach the levels achieved by training accuracy. The training was concluded once improvements in model performance stagnated.

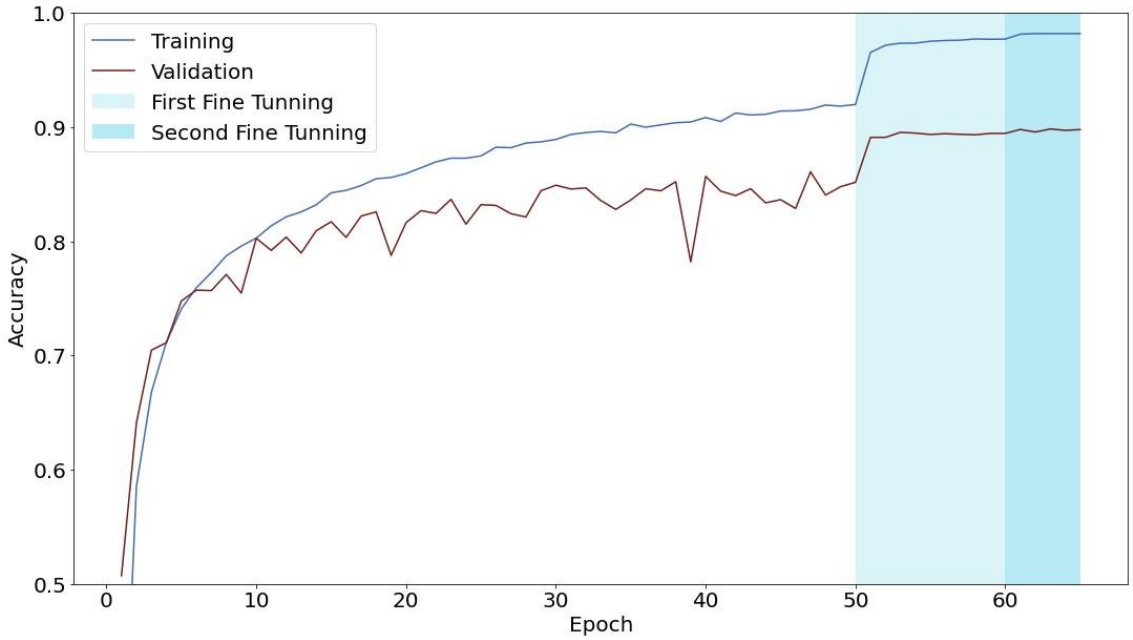


Figure 3:
The CNN Model Training and Test Accuracy

The systematic and comprehensive data generation process enabled the CNN model to effectively learn and accurately detect and quantify sediment accumulation in wastewater collection systems.

4. CNN MODEL VERIFICATION

Model verification was performed using both simulated and experimental data to ensure its accuracy and reliability. The simulated data provided comprehensive conditions to test the model's ability to predict under different physical environments, while the experimental data validated its performance under real-world conditions. This dual approach allowed for comprehensive evaluation, highlighting the model's strengths and identifying potential areas for improvement.

4.1. CNN Model Verification on Simulated Test Plots

A total of 1,829 test plots, generated using SWMM model results and excluded from the training process, were used to assess the quality of the trained model. These plots were systematically selected as every 41st plot from the scatter plot dataset to include diverse physical conditions. Table 3 summarizes the CNN model's prediction accuracy for these test plots. Lower Cross-Entropy Loss values signify improved agreement between predicted and actual values, while an Accuracy (calculated as the ratio of correct predictions to total predictions) near 1 reflects the model's high reliability in predicting exact sediment depth. These metrics were computed for each plot and averaged across 1,829 plots.

Table 3. CNN Model Accuracy for Test Plots

Training	Cross-Entropy	Accuracy	Precision*	Recall*
Main Training	0.559	0.845	0. 855	0. 846
First Fine Tune	0.488	0.884	0. 887	0. 885
Second Fine Tune	0.486	0.891	0. 893	0. 892

** Weighted equally (macro) throughout prediction classes*

The results in Table 3 indicate that the accuracy of the CNN model with test plots is comparable to the training and validation results shown in Figure 3, highlighting a clear distinction between the training, validation, and testing datasets.

Table 4. CNN Model Prediction Ability for Test Plots

Maximum Allowed Prediction Deviations	Example Correct Values for 1 cm Silt Depth Prediction	Number of Correct Predictions	Accuracy
10%	Between 0.9 and 1.1	1,813	0.991
5%	Between 0.95 and 1.05	1,797	0.982
0%	Only 1 cm	1,630	0.891

The second fine-tuned CNN model was evaluated on 1,829 validation plots to predict sediment depth, with the results summarized in Table 4 and depicted in Figure 4. Achieving 0.99 accuracy (for solid content predictions with deviations of up to 10%) demonstrates the model's remarkable success, especially considering that even experts would find it challenging to make predictions with such precision using these plots. An accuracy margin of 10% for solid content predictions is considered acceptable for practical engineering decisions, as it reflects the level of uncertainty that professionals typically tolerate in real-world applications.

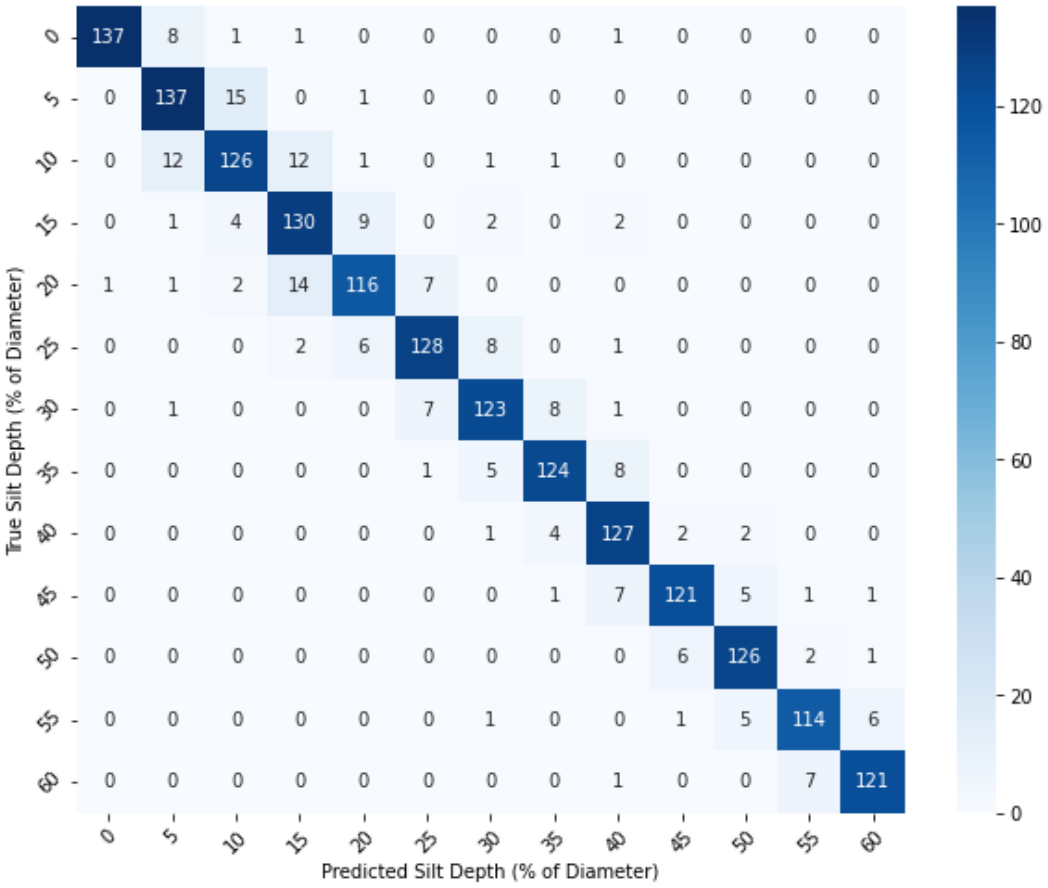


Figure 4:
Confusion Matrix for Test Plots

Figure 4 presents the confusion matrix for the test plots. The predicted values are largely concentrated along the diagonal, indicating that even when the CNN model makes incorrect predictions, the estimated silt depths are generally close to the actual values. One notable exception is a case where an actual silt depth of 0% was predicted as 40% of the pipe diameter. This discrepancy may be due to the input scatter plot points (used by the CNN model) being densely clustered within a broad axis range. Overall, these results align with Table 4, which shows that 99% of the model's predictions fall within a 10% error margin.

However, it is important to note that these results are based solely on SWMM model simulations and will be validated against real-world experimental measurements in the next subsection.

4.2. CNN Model Verification on Real-World Experiments

The study by Enfinger and Kimbrough (2004) presented three experimental results obtained at the hydraulic testing facilities of Accusonic Technologies in Falmouth, Massachusetts. These experiments were designed to replicate real-world conditions, with the laboratory setup simulating hydraulic scenarios typical of urban sewer systems, including blockages caused by large, graded materials such as paper, hygiene products, foreign objects, and plant roots. In each test, an obstruction was placed within the pipe, and flow was introduced by activating a pump. Once the system reached equilibrium, flow depth and volume were measured at three consecutive one-minute intervals. A stainless-steel ruler was used to measure flow depth within the pipe, while an electromagnetic flow meter recorded the flow volume in

the force main. These measurements were then used to calculate flow velocity in the test pipe using the Continuity Equation.

Figure 5 illustrates data from three experiments which are critical for accurately identifying silt depth. In all three experiments, the conduit size (thick gray line) and slope (red line) remained constant (20 cm and 0.72 %, respectively), while the level of blockage at the sensor location varied. Experiment 1 featured no blockage, experiment 2 included a 3.7 cm blockage, and experiment 3 had a 7.5 cm blockage, resulting in distinct variations in the plotted data.

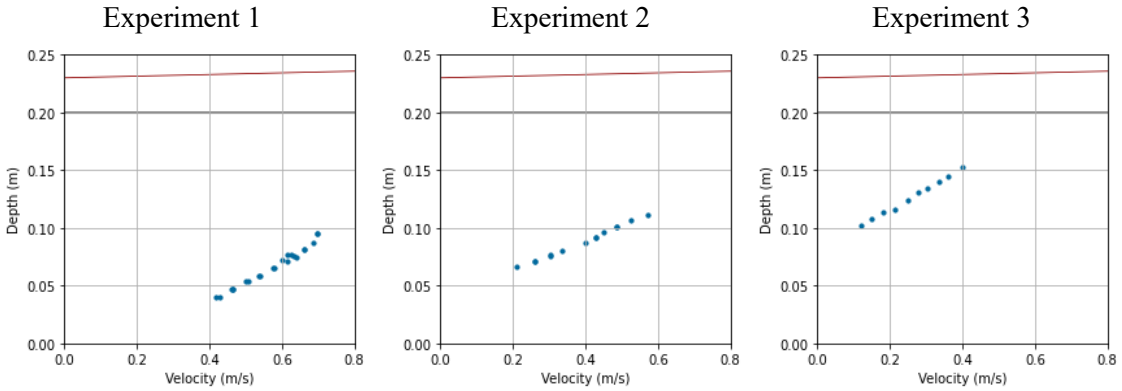


Figure 5:
Real-World Experiments

The labels, numbers, and coordinate lines were removed, and the x and y axis ranges were matched to those of the relevant CNN training figures, as shown in Figure 2. In addition, the resolution of the figures was reduced to 126×123 pixels to align with the CNN model's input structure. The CNN model was then run with these inputs. Table 5 compares the actual blockage values at the sensor location to the predicted silt depths. The blockages were predicted with deviations of 0 cm, 0.3 cm, and 1.5 cm from the actual conditions in Experiments 1, 2, and 3, respectively. Although the SWMM model simulated silt depths uniformly at the bottom of all conduits, the CNN effectively predicted the single-point blockage at the sensor location.

Table 5. Real-World Experiment Results

Experiment	Blockage (cm)	Predicted Silt Depth (cm)
1	0.0	0.0
2	3.7	4.0
3	7.5	6.0

The slight prediction discrepancies from the actual blockage can be attributed to three factors:

- **Manual Data Extraction:** The data for Experiments 1, 2, and 3 were manually extracted from the figures in the original paper, which may have introduced some human error. Furthermore, the number of data points obtained was fewer than originally reported.

- **Model Setup Differences:** Our SWMM model simulated silt distributed uniformly along the entire pipe, whereas the paper experiments placed blockages located immediately after the measurement points.

- **CNN Model Limitations:** The CNN model's predictions are limited to 13 predefined percentages of the pipe diameter as silt depth values. It selects the closest percentage and converts it into the corresponding silt depth. For example, in a 20 cm conduit, the CNN model could only identify silt depths of 3 cm and 4 cm (representing 15% and 20% of the conduit diameter, respectively – see Table 1 variable values). For Experiment 2, the model predicted 4 cm as the closest value.

Despite these factors negatively impacting model performance, the predictions were still accurate for Experiments 1 and 2, with only a slight deviation in Experiment 3. Given the limited availability of tools and research for detecting blockages and silt in collection systems, these results are highly encouraging.

5. CONCLUSION

A CNN model was trained and validated on 82,482 depth–velocity scatter plots generated from 1,482,000 SWMM simulations. The CNN achieved 99% accuracy within a 10% error margin on test plots, demonstrating robust capability to predict sediment accumulation in wastewater collection systems under varying physical conditions. This finding presents a promising tool for improving maintenance and operational efficiency in critical infrastructure.

Further evaluation was conducted on three real-world experiments with a 20 cm conduit size and 0.72% slope and 3 different blockages at the sensor location. The model predicted blockages within 0 cm, 0.3 cm, and 1.5 cm of actual conditions. The 0.3 cm difference is attributed to limitations in the CNN setup stemming from finite computing resources, while the 1.5 cm difference arises from manual data collection, SWMM model setup variations, and CNN-related factors. These results underscore the potential of CNNs for real-time prediction of blockages and sediment accumulation in collection systems, offering a faster and more accurate alternative to traditional methods.

Adopting this technology could transform maintenance practices by enabling proactive responses to potential issues, reducing the likelihood of unexpected failures, and optimizing resource allocation. The improved speed and precision align with the growing demand for smarter, more resilient infrastructure solutions. Nonetheless, further research is needed to fully realize the potential of CNNs in this domain. Future work should focus on refining the model to handle more complex real-world scenarios, enhancing adaptability to diverse system configurations, and expanding applicability across a broader range of operating conditions. These efforts will be critical to transition from promising results in controlled settings to impactful, real-world deployments.

ACKNOWLEDGMENT

I sincerely thank the Inonu University Scientific Research Projects (BAP) unit for their valuable support of this study, which was funded under the BAP project code FBA-2023-3284.

CONFLICT OF INTEREST

The author confirms that there are no known conflicts of interest or common interests with any organization or person.

AUTHOR CONTRIBUTION

There is only a single author for this study.

REFERENCES

1. Berggren, M., Pettersson, T., and Eriksson, E. (2012). Modeling urban flooding under extreme conditions, Water Resources Management, 26(2), 431-442. doi:10.1007/s11269-012-0158-3.
2. Ebtehaj, I., Azimi, H., and Bonakdari, H. (2015). Numerical analysis of sediment transport in sewer pipe, International Journal of Engineering, 28(11), 1564-1570.
3. El-Zaemey, A. K. S. (1991). Sediment transport over deposited beds in sewers (Doctoral dissertation, Newcastle University).
4. Enfinger, K. L., and Kimbrough, H. R. (2004). Scattergraph principles and practice: A comparison of various applications of the Manning equation. *Pipeline Engineering and Construction: What's on the Horizon?*, 1-13.
5. Faris, N., Zayed, T., Aghdam, E., Fares, A., and Alshami, A. (2024). Real-Time sanitary sewer blockage detection system using IoT, *Measurement*, 226, 114146.
6. Ghani, A. A. (1993). Sediment transport in sewers (Doctoral dissertation, Newcastle University).
7. Goodfellow, I., Bengio, Y., and Courville, A. (2016). *Deep learning*. MIT Press.
8. Guo, W., Soibelman, L., and Garrett Jr, J. H. (2009). Automated defect detection for sewer pipeline inspection and condition assessment, *Automation in Construction*, 18(5), 587-596.
9. Khan, A., Sohail, A., Zahoora, U., and Qureshi, A. S. (2020). A survey of the recent architectures of deep convolutional neural networks. *Artificial intelligence review*, 53, 5455-5516.
10. Krizhevsky, A., Sutskever, I., and Hinton, G. E. (2012). Imagenet classification with deep convolutional neural networks, *Advances in Neural Information Processing Systems*, 25.
11. LeCun, Y., Bengio, Y., and Hinton, G. (2015). Deep learning, *Nature*, 521(7553), 436-444.
12. Li, N., Wang, X., Li, Z., Zhao, F., Nair, A., Zhang, J., and Liu, C. (2023). Real-time identification and positioning of sewer blockage based on liquid level analysis in rural areas, *Processes*, 11(1), 161.
13. Li, T., Tan, Q., and Zhu, S. (2010). Characteristics of combined sewer overflows in Shanghai and selection of drainage systems, *Water and Environment Journal*, 24(1), 74-82.
14. Manning, R. (1891). On the flow of water in open channels and pipes, *Transactions of the Institution of Civil Engineers of Ireland*.
15. Montes, C., Vanegas, S., Kapelan, Z., Berardi, L., and Saldarriaga, J. (2020). Non-deposition self-cleansing models for large sewer pipes, *Water Science and Technology*, 81(3), 606-621.
16. Muttil, N., Nasrin, T., and Sharma, A. K. (2023). Impacts of extreme rainfalls on sewer overflows and WSUD-based mitigation strategies: A review, *Water*, 15(3), 429.
17. Perrusquia, G. S. (1992). An experimental study on the transport of sediment in sewer pipes with a permanent deposit, *Water Science and Technology*, 25(8), 115-122.
18. Raschka, S., and Mirjalili, V. (2019). Python machine learning: Machine learning and deep learning with Python, scikit-learn, and TensorFlow 2. *Packt Publishing Ltd*.
19. Rawat, W., and Wang, Z. (2017). Deep convolutional neural networks for image classification: A comprehensive review. *Neural computation*, 29(9), 2352-2449.
20. Regulation on Wastewater Collection and Disposal Systems. (2017) https://webdosya.csb.gov.tr/db/altyapi/icerikler/6-ocak-2017-cuma-20180215122614.pdf
21. Semadeni-Davies, A., Hernebring, C., Svensson, G., and Gustafsson, L. G. (2008). The impacts of climate change and urbanisation on drainage in Helsingborg, Sweden: Suburban stormwater, *Journal of Hydrology*, 350(1-2), 114-125.

22. Stevens, P. L., and Sands, H. M. (1995). Sanitary sewer overflows leave telltale signs in depth-velocity scattergraphs, *Seminar Publication–National Conference on Sanitary Sewer Overflows*.
23. Tan, Y., Cai, R., Li, J., Chen, P., and Wang, M. (2021). Automatic detection of sewer defects based on improved You Only Look Once algorithm, *Automation in Construction*, 131, 103912.
24. Türk, T., Kuşkonmaz, H., and Karadağlı, F. (2022). Atıksu toplama sistemlerindeki işletme problemlerinin tanımlanması, *Uludağ Üniversitesi Mühendislik Fakültesi Dergisi*, 27(1), 205-218.
25. Vitorino, D., Coelho, S. T., Santos, P., Sheets, S., Jurkovac, B., and Amado, C. (2014). A random forest algorithm applied to condition-based wastewater deterioration modeling and forecasting, *Procedia Engineering*, 89, 401-410.
26. Vongvisessomjai, N., Tingsanchali, T., and Babel, M. S. (2010). Non-deposition design criteria for sewers with part-full flow, *Urban Water Journal*, 7(1), 61-77.
27. Xie, Q., Li, D., Xu, J., Yu, Z., and Wang, J. (2019). Automatic detection and classification of sewer defects via hierarchical deep learning, *IEEE Transactions on Automation Science and Engineering*, 16(4), 1836-1847.